



## Seismic response of random rubble stone masonry buildings from mid-hills of central Nepal

Rabindra Adhikari<sup>1,2\*</sup>, Ayush Raj Shrestha<sup>1</sup>, Anu Aryal<sup>1</sup>, Binaya Sharma<sup>1</sup>, Abhishek Budhathoki<sup>1</sup>, Bhawana Bhatt<sup>1</sup>, Biplov Bhandari<sup>1</sup>

<sup>1</sup> Department of Civil Engineering, Thapathali Campus, Institute of Engineering, Kathmandu, Nepal

<sup>2</sup> Department of Civil Engineering, Pulchowk Campus, Institute of Engineering, Kathmandu, Nepal

\*Corresponding email: rabindraadhi@gmail.com

Received: April 30, 2024; Revised: June 06, 2024; Accepted: June 08, 2024

doi: <https://doi.org/10.3126/joeis.v3i1.65330>

### Abstract

Rubble stone masonry in mud mortar is the most prevalent stone masonry buildings in the mid-hills accounting for more than 70% of Nepali building stock. However, these types of construction are relatively more vulnerable to seismic events. Interestingly, some of these masonry buildings performed very well while many others collapsed. For a detailed understanding of performance of these masonry at component level during earthquake excitation, this paper presents the gradual failure mechanism for a typical stone masonry from mid-hills of central Nepal. The analysis was carried out by first linear analysis of Finite Element macro-model, followed by non-linear push-over analysis using finite element method and equivalent frame method. Performance was assessed under different levels of earthquake. Linear analysis results showed that these masonry buildings satisfy the drift requirements as per Nepal building code with adequate margin but are susceptible to heavy damages, especially in shear along with significant compression crushing and tensile cracks, under design level earthquake. Detailed non-linear analysis showed that the building attains performance states of immediate occupancy, life-safety, and collapse prevention at peak ground intensities of 0.175 g, 0.25 g and 0.295 g, respectively, while the analysis using equivalent frame model showed the performance at peak ground acceleration intensities of 0.15 g, 0.19 g and 0.3 g, respectively. The existing damage in the building with partial collapse of gable due to 2015 Gorkha earthquake with estimated exposed ground intensity of 0.18 g is well predicted by the analysis.

**Keywords:** Damage mechanism; equivalent frame model, seismic performance, stone masonry.

### 1. Introduction

Stone masonry structures can mainly be seen and spotted in the rural parts and the mid-hills of Nepal. Seismic risk is high in Nepal with potential loss of life and property (Bhochhibhoya & Maharjan, 2022). The high seismicity of Nepal is related to the presence of active faults between tectonic plates along the Himalayas, such as the Main Boundary Fault (MBF) and Main Central Thrust (MCT) (Paudel & Pradhan,

2010). Not only large magnitude earthquakes but even small magnitudes of earthquake, frequently occur (S. S. Khadka, 2018). Some notable seismic events in the past include a devastating earthquake of  $M_w$  7.8 with epicenter at Barpak, Gorkha. One of the major causes of structural failure is its improper design without following engineering and architectural guidelines (Adhikari et al., 2023). Mainly in old practices, the stone masonry structures were built without much focus and consideration of seismic loading that can act upon the structure. The practice still exists in most of the rural parts of Nepal (B. Khadka & Shakya, 2021). Even many of the new constructions in remote areas include several construction defects that challenges the seismic response of such masonry buildings (Adhikari, 2023).

Mud has been, and continues to be, the most widely available and used building material throughout most developing countries. Nepal have been suffering a lot with lots of casualties and house damages by the earthquake (B. Khadka & Shakya, 2021). Total number of houses in Nepal is 6,660,841, out of which 2,042,978 are made of brick or stone masonry with mud mortar (BM/SM) in outer walls (NPHC, 2021). Most Unreinforced Masonry uses mud as binding material which has relatively poor capacity to bind stones together. More casualties in the 2015 earthquake were from the collapse of URM structures, mostly rubble stones (Pokharel et al., 2015). This study considers stone masonry of Bethanchowk village Kavre district where about 50% of the building are masonry buildings (NPHC, 2021).

Study of these type of traditional construction systems is often overlooked considering outdated technologies. However, such structures are present in abundant quantity in the country, and still being constructed in various parts of the country as a well-known construction system with local materials and local masons using local knowledge. But many of such constructions do not follow the prevalent seismic code and engineering guidelines leading to high risk of collapse during seismic events. Recent seismic activities occurring in the country have also brought attention to the public and the related authorities for the further study of the performance of such structures, and necessary intervention to existing structures. Government of Nepal has endorsed some changes in stone masonry construction system in Nepal such as preparation of design catalogues and revision of few NBCs in 2015 by Department of Urban Development and Building Construction (DUDBC). However, the extent of their earthquake safety is still not well defined (Gautam, et al., 2021). Static and dynamic analysis can contribute greatly to understanding the behavior of buildings, but at the same time, uncertainty encapsulated within material properties in masonry buildings has pronounced effect on the dynamic response of the building (Aish et al., 2017).

This study investigates the construction system of typical stone masonry buildings commonly built in mid-hills of central Nepal, particularly from Kavre district in Bagmati Province. A two-storey plus attic building was geometrically measured in detail, and ambient vibration was also measured using a highly sensitive three-axis accelerometer to determine its dynamic characteristics. Two plus attic buildings being the most common geometry in buildings of central Nepal, it was selected for detailed numerical modeling and analysis to determine its damage mechanism. The result of this analysis is useful in understanding the static and dynamic characteristics of such stone masonry under seismic loading. This understanding also helps in evaluating various strengthening measures for existing vulnerable structures and provides insights for design of new structures for better seismic resilience.

## 2. Materials and Methods

### 2.1 Building description

Based on visual investigation of several buildings in the village of Bethanchowk, for the detailed numerical model, a two-storey plus attic building was selected representing the most common geometry and construction system and structurally isolated from adjacent buildings.

The field visit was made to Dhunkharkha, Bethanchowk of Kavre district (Figure 1), which is about 12.9 km from Panauti Buspark, in December 2023, to record the construction system, damage pattern, and dynamic properties of a few mud-mortar stone masonry buildings of the site. A typical stone masonry building, which has a floor area of 39.40 square meters, made of mud mortar as shown in Figure 2 was selected and studied in detail. The total height of the building up to attic level is 6.90 m. Height of the first storey is 2.14 m, height of the second storey is 2.230 m, and that of the attic is 2.53 m (including 1.23 m height of rectangular part and 1.30 m height of triangular or gable).



**Figure 1:** Location map of the study building (*Google Maps*)



**Figure 2:** Left side-view (left) and front-view (right) of the study building

Figure 3 shows the plan of the building and Figure 4 shows the elevations of the building. From our observation at site, most of the buildings at Bethanchowk have no opening at back, and rare openings at the sides on the ground floor and attic. Most of the openings were observed in the front side. In Hilly terrain, such types of buildings are mostly observed in significant numbers. This building is free from attachment to soil on either side.

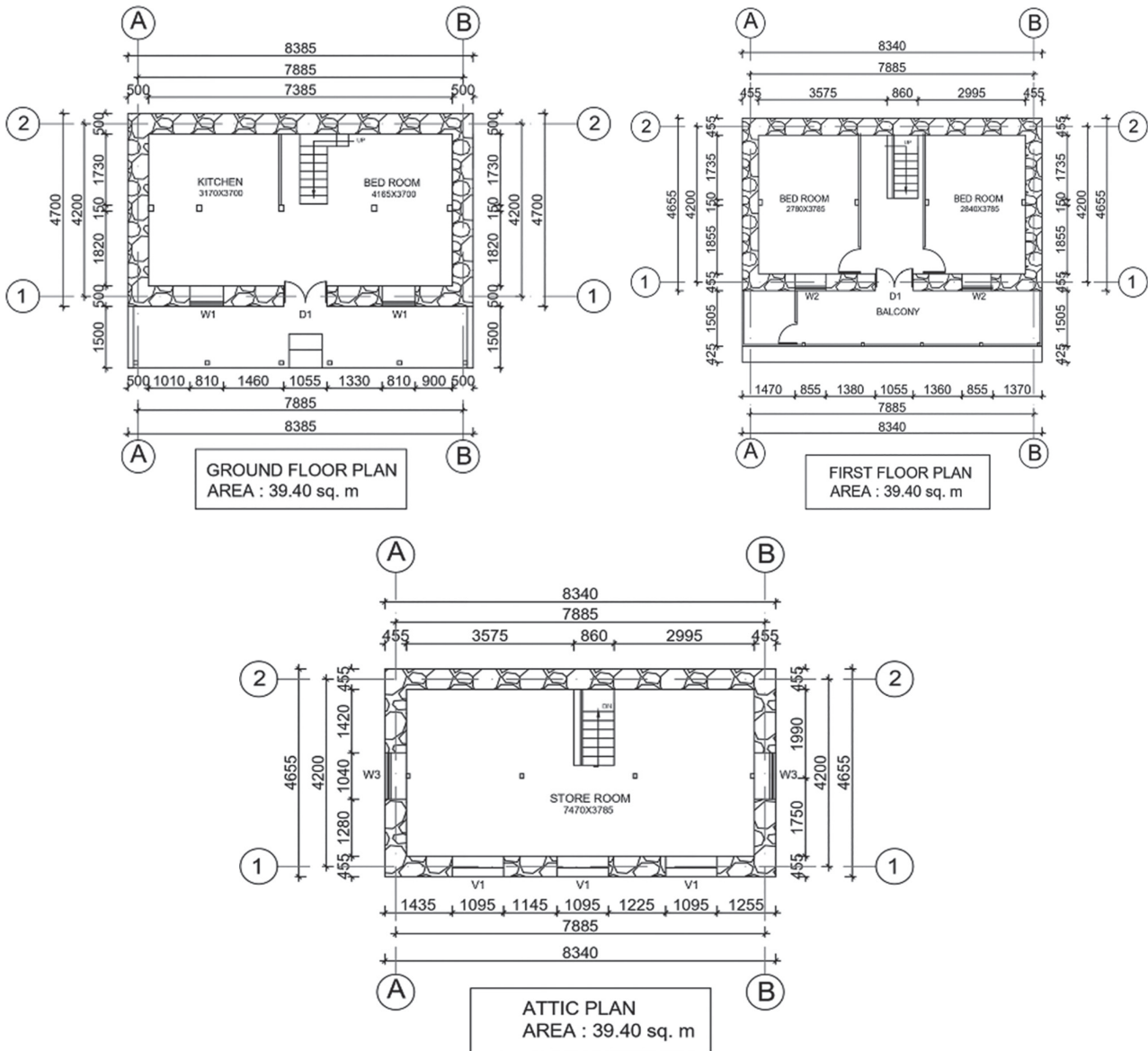
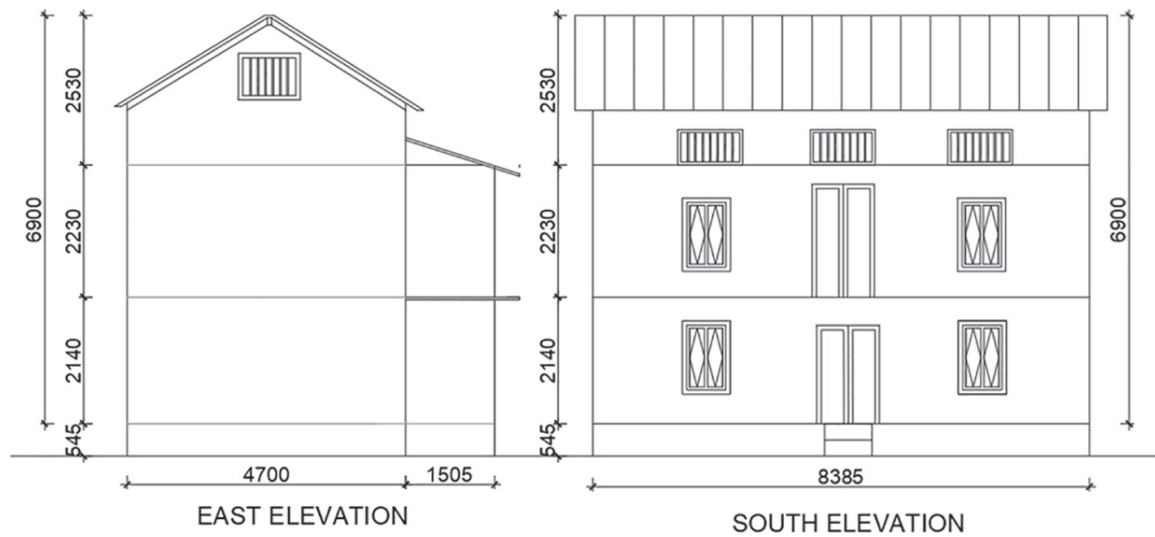


Figure 3: Plan of the study building



**Figure 4:** Left (left) and front (right) elevation of the study building

## 2.2 Dynamic system identification of the building

Depending on the mechanical characteristics of the building material, the geometry of the building, and the structural and connection system, every building vibrates at its natural period, attributed to the mass and stiffness of the building as a whole and different components. As all buildings are excited with low amplitude white noise in ambient conditions, the ambient vibration response can be recorded and processed to determine the natural period of vibration and damping ratios. Thus, a highly sensitive tri-axial accelerometer was placed on the upper floor of the selected building and the ambient vibration measurement data was recorded for an interval of 30 minutes. The data was further processed for the dynamic system identification of the building, especially the determination of natural periods and corresponding damping.

System identification, also called experimental modal analysis, is a mathematical framework conducted to identify dynamic properties of structures from the measured vibration response record of the structures (Dhakar, 2020). Blind system identification was conducted in current experiments which means that the system identification is done based on response only without any consideration of the excitation. One of the most widely appreciated algorithms for modal analysis using vibration records is the Numerical Algorithm for Subspace State Space System Identification (N4SID). This method is based on a mathematical model called state-space model which consists of a set of input, output and state variables linked together by first order differential equations. The N4SID algorithm is used together with fourth-order Butterworth filtration and Tukey window tapering. Band pass filters can only be used if the analyst is certain to the range of frequency, which is not possible explicitly, so, pass band based higher order filters are required for ambient vibration time series.

## 2.3 Numerical analysis

The detailed numerical analysis was conducted using two approaches. In the first approach, a finite element model was prepared in SAP2000v24. A three-dimensional finite element model (FEM) is shown in Figure 5. The structure was assumed to be fixed at support. The walls were idealized as shell elements whereas the flexible timber and mud floor slabs were not modeled. Instead, the loads on the floor were calculated and applied to the Dalins (timber beams). Similarly, load on the roof including the roofing sheets were calculated

and applied on the purlins. Linear elements such as Nidals (large timber girder supporting Dalins), Dalins, Tham (vertical timber posts), Dada (roof-rafters), and Bhatas (roof-purlins) were idealized as frame elements.

Free vibration analysis of the structure was carried out using eigenvector analysis to identify the modal periods and frequencies (Adhikari et al., 2023) reported that there is notable change in response of the building when the elastic modulus of stone masonry varies significantly which is common in case of mud-mortared building. Such variations are observed due to variation in moisture content in the mud mortar, the type of clay used as mortar, stone laying patterns, past damages, among others. Further, mud mortared buildings tend to show high stiffness in low amplitude vibrations such as ambient vibration while lower stiffness in high amplitude vibration or large-scale deformation, as observed in several experimental campaigns (Adhikari & D'Ayala, 2019) (Kumar Bothara et al., 2023).

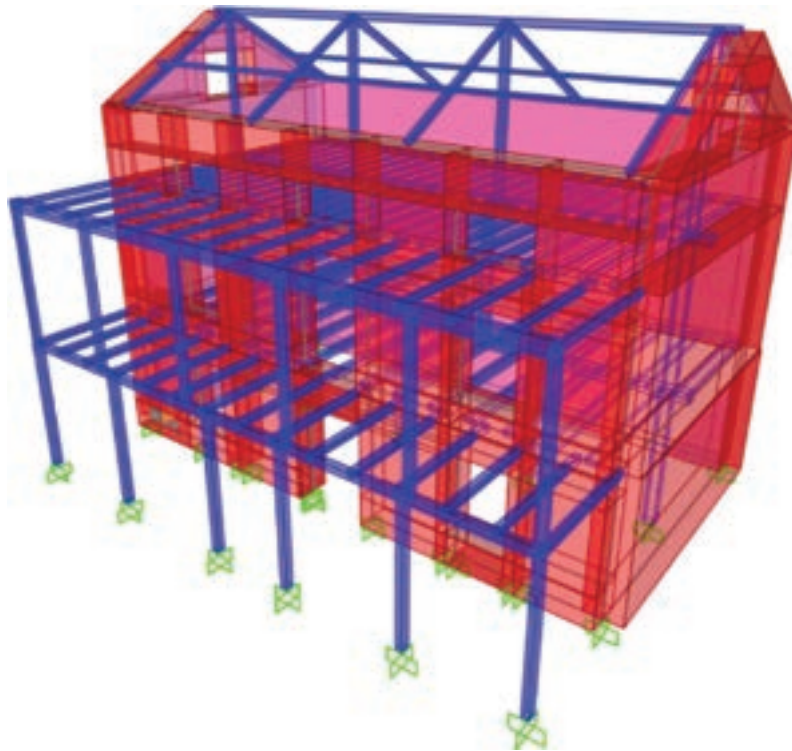


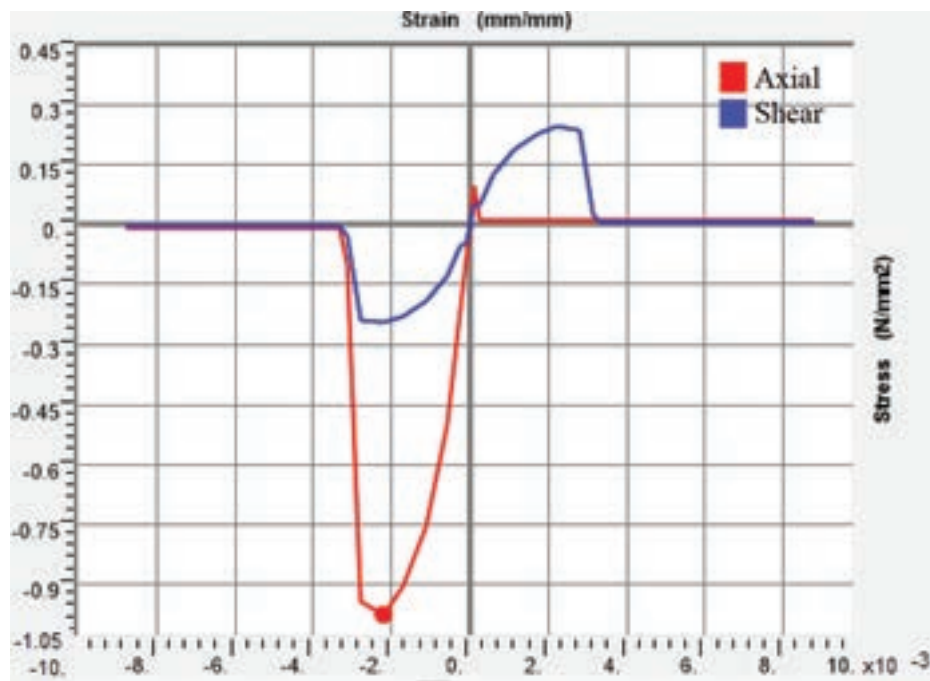
**Figure 5:** FEM model of the building in SAP2000

The structure was analyzed as per NBC 105:2020 (DUDBC, 2020) by considering various structural elements, loadings, boundary conditions and all other constraints and the model is simulated. Design dead loads and design live loads were applied in the model in accordance with IS 875-1, 1987 (BIS, 1987a) and IS 875-2, 1987 (BIS, 1987b) respectively. The earthquake load was determined based on NBC 105:2020 (DUDBC, 2020) Considering soil type B (based on visual soil classification per NBC 105:2020 (DUDBC, 2015)) and unreinforced masonry (ductility factor of 2 and overstrength factor of 1.2), the base shear coefficient was calculated to be 0.365 with a base shear of 493.346 kN. Since the height of the considered house is less than 15 m, linear analysis was carried out by using an equivalent static method only to understand the design forces in par with NBC 105:2020 (DUDBC, 2020). Drift check, displacement check, modal period and mode participation factor, and stresses (compressive, tensile and shear) were evaluated and compared to the respective permissible values. The material properties used in the analysis are presented in Table 1.

**Table 1:** Material Properties used in FEM and EFM models.

Parameter	Value	Reference
$\gamma_{\text{masonry}}$	21.57 KN/m <sup>3</sup>	IS 875-1, 1987 (BIS, 1987a)
$E_{\text{masonry}}$	245.11 MPa	Adhikari & D'Ayala (2019)
$\mu_{\text{masonry}}$	0.25	Adhikari & D'Ayala (2019)
$\gamma_{\text{timber}}$	5.005 KN/m <sup>3</sup>	IS 883: 1994 (BIS, 1994)
$E_{\text{timber}}$	6800 MPa	IS 883: 1994 (BIS, 1994)

To further understand the post-elastic behaviour of the building, non-linear analysis was conducted using the same FEM in SAP2000 using non-linear stress-strain model of the masonry as presented by (Adhikari & D'Ayala, 2019). However, to account for poor quality of construction and low strength of commonly built masonry, the presented stress-strain is scaled to match the peak strength of masonry to be 1 MPa, and peak tensile strength is considered as 10% of compressive strength as presented in Figure 6.

**Figure 6:** Stress strain curve of stone masonry adopted in the study

In the second approach, equivalent frame model was prepared using a professional Italian software PRO\_SAP with PRO\_SAM Plug-in. A three-dimensional Equivalent Frame Model (EFM) is shown in Figure 7. The walls are modeled as a SAM wall element fundamentally used for non-linear static pushover analysis. The SAM wall element is further divided into spandrels and piers. The intersecting area of piers and spandrels are commonly considered rigid in the EFM and are defined as a rigid element. The linear elements such as timber joists, Nidal, Dalin, Thams, roof-rafters, and roof-purlins were modeled as SAM-D2 elements (frame elements).

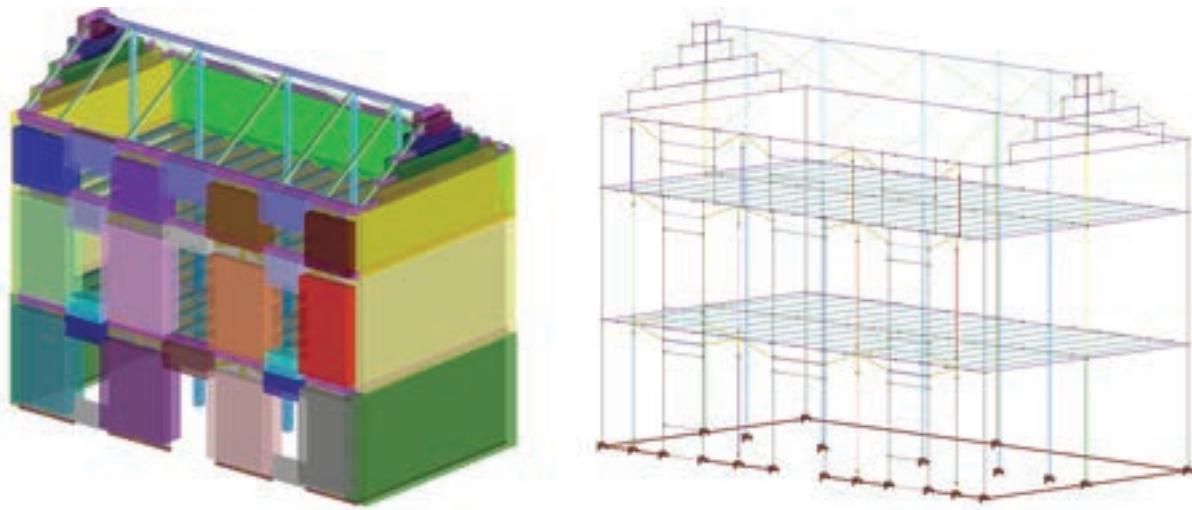


**Figure 7:** EFM model of the building (Solid view (left) and Equivalent frame view (right))

This study includes static non-linear analysis for a rigorous study of structures to have insight on the post-yield performance of the structure. The seismic parameters were adjusted to have the seismic force matching that calculated from NBC 105:2020 (DUDBC, 2020) such that the base shear coefficient calculated based on NBC 105:2020 (DUDBC, 2015) as used in the FEM model in SAP2000v24 match with that in PRO\_SAP model. The base shear (force) distribution was considered to be a triangular distribution as in linear static according to par. 7.3.3.2 of NTC 2018 (MIT, 2018). The material properties used in the model includes the unit weight of masonry ( $\gamma_{\text{masonry}}$ ), Poisson's ratio of masonry ( $\mu_{\text{masonry}}$ ), unit weight of timber ( $\gamma_{\text{timber}}$ ), and Young's modulus of elasticity of timber ( $E_{\text{timber}}$ ) which is summarized in Table 1.

### 3. Results and Discussion

Free vibration analysis was conducted to observe the natural periods for various modes. Then seismic analysis was conducted as per Nepal building code to determine the demand stresses in various components that estimates the damage pattern in the masonry. To further strengthen the understanding of damage, the analysis is extended to non-linear push over analysis using the same FEM but with non-linear stress-strain relationship for the masonry walls. Finally, an equivalent frame model was prepared in PRO\_SAP for the rubble stone masonry building, and the damage sequence was determined on incremental horizontal load.

#### 3.1 Free vibration responses

Free vibration analysis was carried out using FEM to determine the natural periods of vibration. Eigen vector analysis was carried out to determine the characteristics of the first few modes. The first mode was lateral translational vibration of building along short direction while second mode was lateral translational vibration of building along long direction, and the third mode is torsional vibration. However, as discussed earlier, the elastic modulus established from experiments or high amplitude deformation are much lower than that expected for low amplitude vibration such as ambient vibration. The observed periods for the first three modes are 0.446 s, 0.312 s and 0.257 s respectively.

The free vibration modes were also established for ambient vibration records of 30 minutes using N4SID method. The 30 minutes data was divided into 10 segments and analyzed with modal order of 12 to obtain

the modal characteristics. The analysis was able to produce modal characteristics up to 8<sup>th</sup> modes in each direction out of which first five are presented in Table 2. The fundamental period was about 0.23 s and 0.22 s in x-direction and y-direction respectively.

**Table 2:** Measured modal characteristics

Mode	Frequency (Hz)		Time period (sec)		Damping Ratio	
	X-dir	Y-dir	X-dir	Y-dir	X-dir	Y-dir
1	4.3528	4.4373	<b>0.230</b>	<b>0.225</b>	0.0447	0.0093
2	8.8758	8.7367	0.113	0.114	0.0308	0.0318
3	11.0657	11.5431	0.090	0.087	0.155	0.0975
4	12.9937	14.3711	0.077	0.070	0.0519	0.0421
5	15.9398	18.72	0.063	0.053	0.0192	0.2189

However, the measured periods are much lower than those observed from FEM. Hence, an attempt was made to update the FEM model by scaling the elastic modulus of the stone masonry to match the measured period. Accordingly, the best match was obtained when the elastic modulus was 1256 MPa which is 5.12 times the elastic modulus of isolated wall determined experimentally (presented in Table 1). This is also in agreement with common specification of modulus of elasticity between 1000 MPa to 2000 MPa (FEMA 356, 2000) and (IAEE, 2014) for elastic analysis of masonry buildings. The (FEMA 356, 2000) also clarifies that the factor 550 for estimation of elasticity is in lower side to account of the higher value of observed compressive strength in lab-tests. This signifies that, for masonry buildings in mud mortar, low amplitude vibration is associated with relatively higher stiffness of the building compared to the experimentally established elastic modulus. Further, the observed stiffness is about double the stiffness as suggested by IS 1893 (Part 1):2016 (BIS, 2016) for masonry wall which was calculated as 550 times the mean strength of masonry.

### 3.2 Elastic response to seismic forces

Elastic analysis was conducted using FEM in SAP2000v24, with seismic force as per NBC 105:2020 (DUDBC, 2020) considering medium soil sites, Type B (visual evaluation). The interest was to observe the stresses in various components of the building to predict the damage mechanism of the building.

#### 3.2.1 Drift and displacement

Drift check was done in accordance with NBC 105:2020 (DUDBC, 2020). The permissible drift ratio is 2.5% for ULS and 0.6% for SLS as per NBC 105:2020 (DUDBC, 2020). As the observed drift of 0.1% in ULS is much less than permissible drift in ULS, and even less than permissible drift for SLS, the drift criteria is well satisfied by the structure. In line with analysis experiences of several other masonry buildings by the authors, the results indicate that drift criteria are well satisfied by typical masonry buildings.

#### 3.2.2 Demand stresses

The linear analysis was conducted in SAP2000v24 to evaluate the stresses subjected on the elements of the building. In normal design procedures, it is common to conduct only linear analysis for the simple residential building for the new or intervention design. This fact can be compared with the results of nonlinear analysis and the stresses observed can be verified by the results of the nonlinear analysis to assess the applicability

of linear analysis for common purposes. The design procedure and load combinations are adopted from NBC 105:2020 (DUDBC, 2020). The masonry wall is observed as a combination of vertical piers and horizontal spandrels.

From the analysis, the compressive stresses were found within reasonably safe limit (0.47 MPa) according to (Adhikari & D'Ayala, 2019) in all the walls due to gravity only load combination (1.2DL+1.5LL) while the compressive stresses due to seismic load combinations (DL+0.3LL±EQ\_X and DL+0.3LL±EQ\_Y) are higher up to about 0.69 MPa with maximum at the extreme corners of the walls, the overstress being extended to about 50% of the pier area. Hence, although the demand compressive stress can be argued to exceed the commonly adopted permissible strength of masonry, it is still much less than maximum compressive strength of about 1 Mpa.

Various stresses observed for the study building is shown in Figure 8 to Figure 10. Figure 8 shows the horizontal stresses ( $S_{11}$ ) observed in the front face of the building corresponding to different PGAs of 0.15g, 0.19g and 0.35g respectively. Similarly, Figure 9 shows the vertical stresses ( $S_{22}$ ) and Figure 10 shows the shear stresses ( $S_{12}$ ) observed in the front face of the building corresponding to different PGAs of 0.15 g, 0.19 g and 0.35 g respectively.

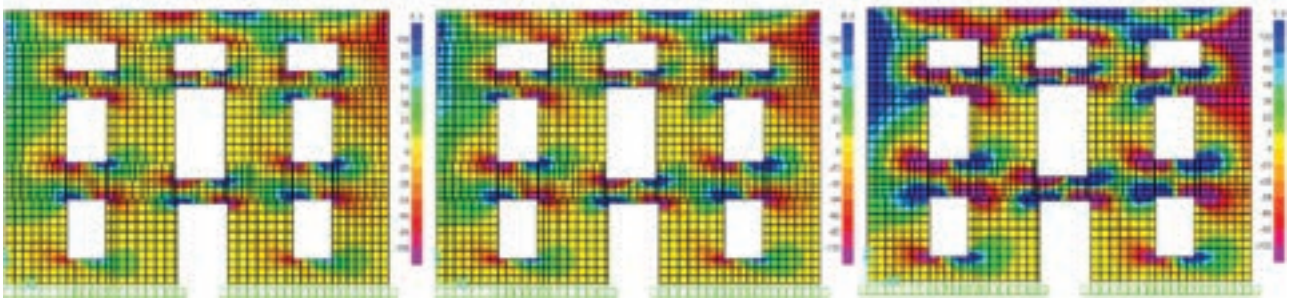


**Figure 8:** Horizontal stresses ( $S_{11}$ ) observed in the front face of the building corresponding to different PGAs of 0.15 g, 0.19 g, 0.35 g (left to right)

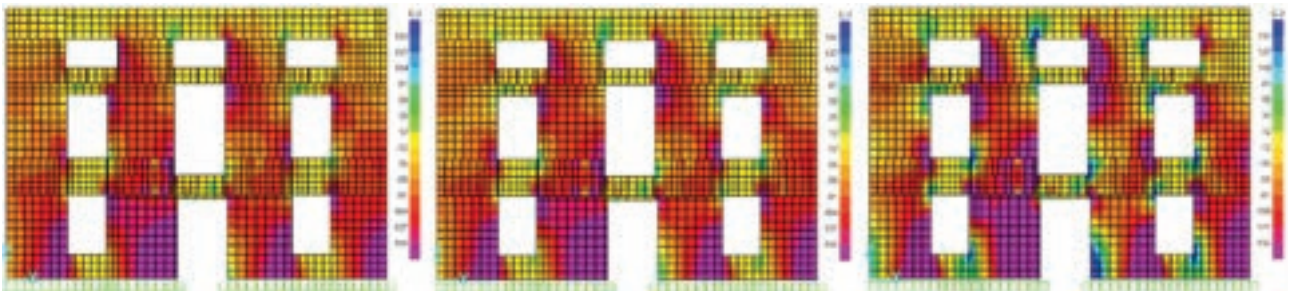


**Figure 9:** Vertical stresses ( $S_{22}$ ) observed in the front face of the building corresponding to different PGAs of 0.15 g, 0.19 g, 0.35 g (left to right)

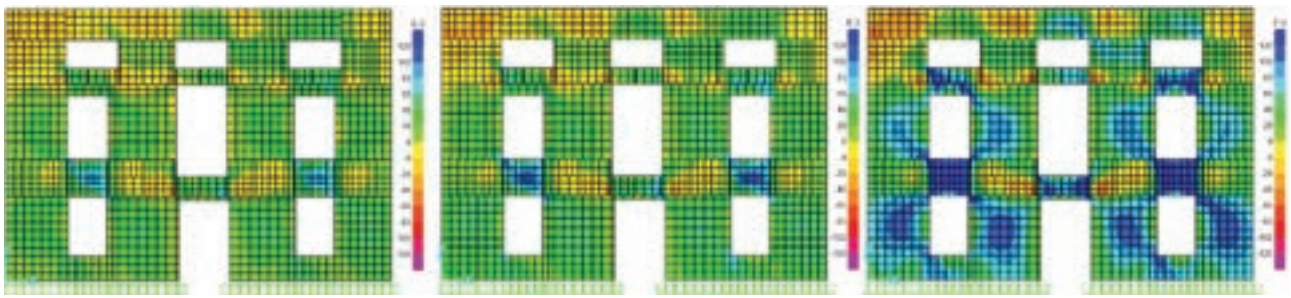


**Figure 10:** Shear stresses ( $S_{12}$ ) observed in the front face of the building corresponding to different PGAs of 0.15g, 0.19g, 0.35g (left to right)

In general, in-plane tension are avoided in masonry design, in par with is 1905:1987 (BIS, 1987c) as well. However, the analysis shows tensile stresses especially at corners of doors, windows, and at extreme corners of walls. Hence, some tensile cracks are expected in the masonry, but once cracks are generated, stresses get redistributed in adjacent portion and no significant damage is generally observed due to this tension. The common design practice to cater to this tension is to provide vertical reinforcements such as steel rebar or timber posts that can integrate the wall even in case of these tensions and can significantly improve the resilience of these walls.

Shear Stresses at piers and spandrels of walls for different combinations of load was determined. Maximum shear is observed to be critical at in-plane loading. The maximum shear stress in wall appeared in the middle portion of the ground floor and the first floor, and the peak stress was about 0.15 MPa, which is higher than commonly specified safe strength of 0.05 MPa for mud-mortared masonry which is in reasonable range if factor of safety is considered to be 2 for the observed shear strength from diagonal test (Kumar Bothara et al., 2023), though within the max shear strength of 0.24 MPa as per the adopted material characteristics as shown in Figure 6. The observed peak stresses are tabulated in Table 3.

**Table 3:** Peak stresses in the masonry wall

Intensity of ground shaking	Horizontal stress ( $S_{11}$ ) at the spandrel between openings of the GF and FF (MPa)	Shear stress ( $S_{12}$ ) at the spandrel (MPa)	Maximum vertical stress ( $S_{22}$ ) at piers (MPa)
0.15 g	0.222	0.09	0.337
0.19 g	0.291	0.115	0.43
0.35 g	0.553	0.211	0.614

Hence, it is observed that the stresses in the masonry under design earthquake exceeds the commonly specified permissible values, though within the experimentally established peak capacities. It justifies that some well-built buildings were able to resist even large earthquakes in the past. However, to achieve this performance, the local failure modes and out of plane collapse of components need to be resisted. Hence, several poorly built buildings collapsed even at intensities lower than 0.15 g due to various deficiencies in the constructions as reported by (Gautam & Chaulagain, 2016).

### 3.3 Non-linear capacity of the building

The building was modeled using FEM in SAP2000v24 with homogenized non-linear stress-strain characteristics of masonry wall using macro model. A detailed model was developed which could capture all the aspects of non-linearity including material nonlinearity as well as geometric nonlinearity. Nonlinear static pushover analysis was used to evaluate the seismic capacity of the existing structure. Non-Linear pushover load cases were initially defined, and the analysis was run using Event-to-Event only solution scheme. In Event-to-Event stepping, the load steps will automatically be subdivided where changes occur in the stiffness of nonlinear elements. This causes a series of nearly linear steps to be taken, which can minimize deviation from equilibrium (CSI (Computers & Structures INC), 2016). The stress-strain curve adopted for the masonry is as shown in Figure 6. A joint at central part of the building at the eaves level of the building was selected as the control node. The capacity curve thus obtained from the analysis for x-direction is as shown in Figure 11.

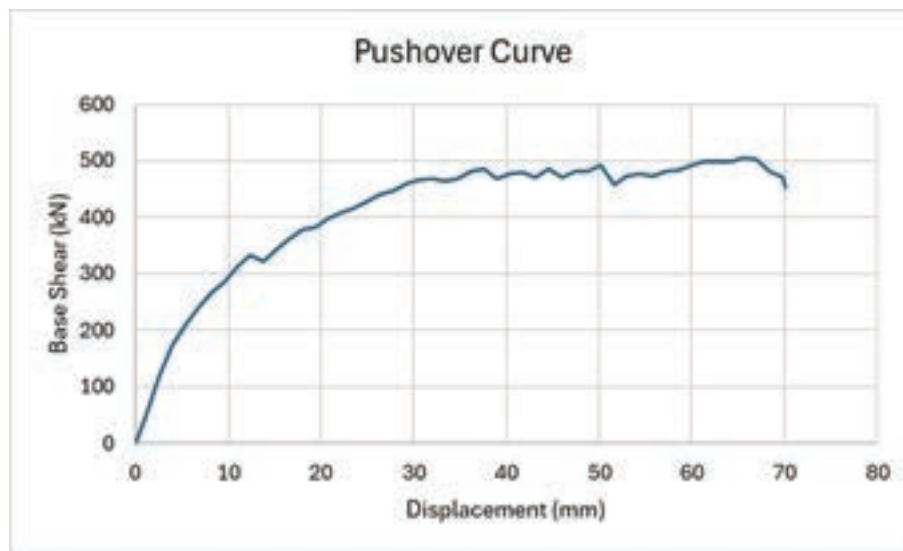


**Figure 11:** Pushover Curve from SAP2000v24

The curve shows significant linearity up to 5 mm displacement of eaves at base shear of about 180 kN. Then, non-linearity was gradually introduced with base shear saturation at about 450 kN with displacement of 30 mm.

Similarly, the structure was again modeled in PRO\_SAP (with PRO\_SAM plugin) using the Equivalent Frame Model for the rubble stone masonry. While the strength of the wall was adjusted as per the adopted material model, the strain characteristics were predefined in the software. Non-linear static pushover analysis in PRO\_SAP was executed, and capacity curve was obtained as in accordance with NTC 2018 (MIT, 2018). The base shear (force) distribution was considered to be a triangular distribution as in linear static according to par. 7.3.3.2 (MIT, 2018). The capacity curve thus obtained with the completion of pushover analysis in PRO\_SAP is shown in Figure 12.

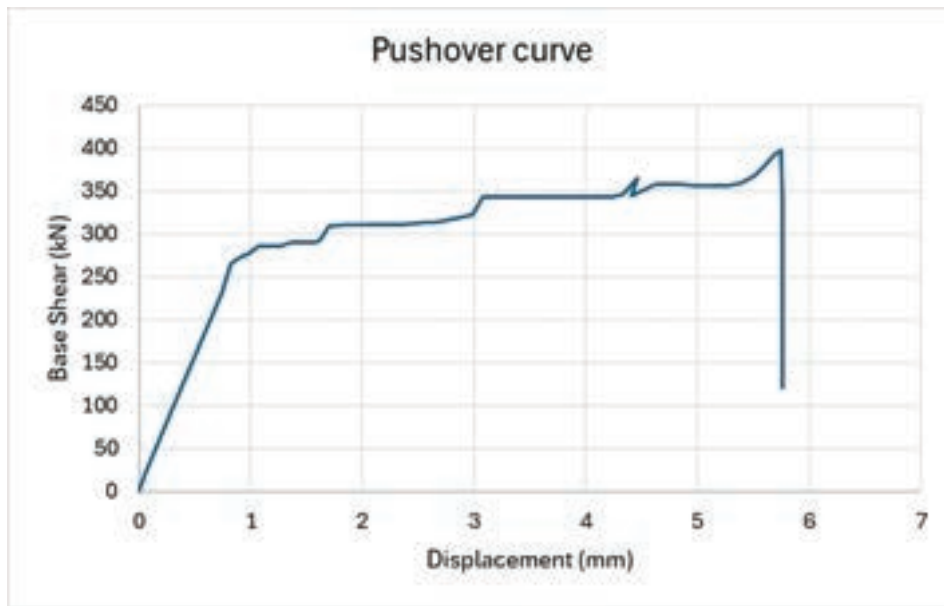


**Figure 12:** Pushover Curve from PRO\_SAP (with PRO\_SAM Plugin)

While the nature of pushover curve from the two approaches are similar, the displacement parameters are significantly different. This is due to the method of analysis adopted in each approach. In FEM, a non-linear material model is provided, which is gradually loaded, and non-linearity is introduced gradually. Out of plane failure and rocking is not considered in the model thus estimating large non-linear capacity.

However, in EFM, force-based analysis is conducted, and different local failure mode of each wall components (spandrels and piers) are considered in line NTC 2018 (MIT, 2018). The masonry component failure is brittle, and hence, significant loss of strength is captured at small deformation. Iterative analysis is conducted to determine forces in different wall components and to estimate their damage states. Further, these failure criteria are based on design principles which account for large factor of safety, and hence indicate failures at lower values of forces. Hence, this type of curve is useful for the design with margins of safety.

Nonetheless, both curves estimate the peak base shear of nearing 400 KN which is quite reasonable and in agreement with each other, at least for the force-based analysis.

### 3.4 Damage pattern and performance of the masonry building

Once the capacity curve is established, different performance states can be defined to characterize the damage of the building. Four performance states (levels) are defined (Lagomarsino & Giovinazzi, 2006) and shown in equations (1) - (4). In order to identify the damage suffered by the buildings, damage limit states  $S_{d,k}$  are directly identified on the capacity curve as a function of the yielding  $d_y$  and of the ultimate  $d_u$  displacements.

$$\text{Immediate Occupancy (IO)} = S_{d,1} = 0.7d_y \dots\dots\dots (1)$$

$$\text{Life Safety (LS)} = S_{d,2} = 1.5d_y \dots\dots\dots (2)$$

$$\text{Collapse Prevention (CP)} = S_{d,3} = 0.5 (d_y + d_u) \dots\dots\dots (3)$$

$$\text{Complete Collapse} = S_{d,4} = d_u \dots\dots\dots (4)$$

Based on the capacity curve obtained from FEM, the performance states are defined as shown in Table 4 and Figure 13.

**Table 4:** Different performance states of the building

Extent of damage	Corresponding to	Damage states	Displacement (mm)	Base shear (KN)
Slight	IO	$S_{d,1}$	9.1	273
Moderate	LS	$S_{d,2}$	19.5	378
Extensive	CP	$S_{d,3}$	31.5	467
Complete	Complete Collapse	$S_{d,4}$	50	490

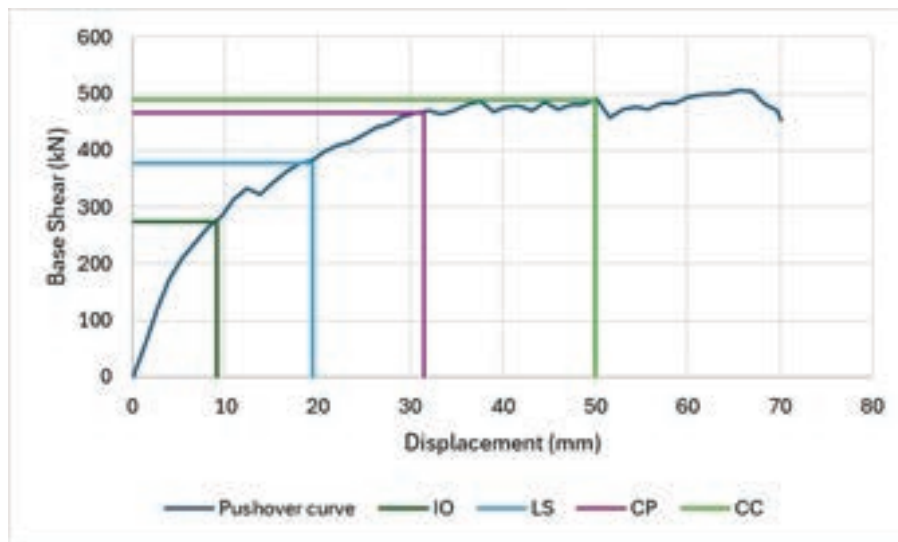


**Figure 13:** Damage states identified on the capacity curve

Accordingly, the performance of the building as a whole is defined. The response spectrum curve corresponding to soil type B adopted from NBC 105:2020 (DUDBC, 2015) is considered as the demand curve whereas the pushover curve is taken as the capacity curve. For the determination of the performance of the building, initially the demand and capacity curves are converted into ADRS format. This is accomplished in accordance with (ATC 40 Seismic Evaluation and Retrofit of Concrete Buildings, 1996). For the conversion of the demand curve, firstly, spectral displacement ( $S_d$ ) for each point the curve is found using  $S_a$  and T.

By using the relation in (ATC 40 Seismic Evaluation and Retrofit of Concrete Buildings, 1996) the base shear is transformed to spectral acceleration and the roof displacement is transformed to spectral displacement using equation (5), equation (6) and equation (7).

$$S_d = \frac{T^2}{4\pi^2} S_a \dots\dots\dots (5)$$

$$S_a = \frac{V_b/W}{M_k/M} g \dots\dots\dots (6)$$

$$S_d = \frac{\Delta_{rooftop}}{P_k \Phi_{k,rooftop}} \dots \dots \dots (7)$$

Accordingly, the performance of the building corresponding to various ground motion intensities of 0.15 g, 0.18 g and 0.3 g are depicted in Figure 14, Figure 15, and Figure 16 respectively and in Table 5.

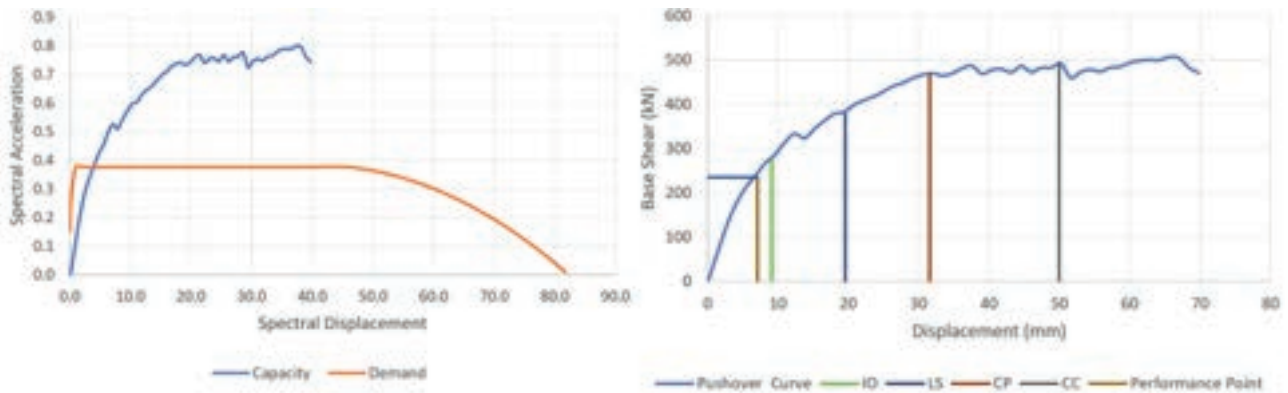


Figure 14: Performance point (left) and performance of the building (right) for 0.15 g PGA

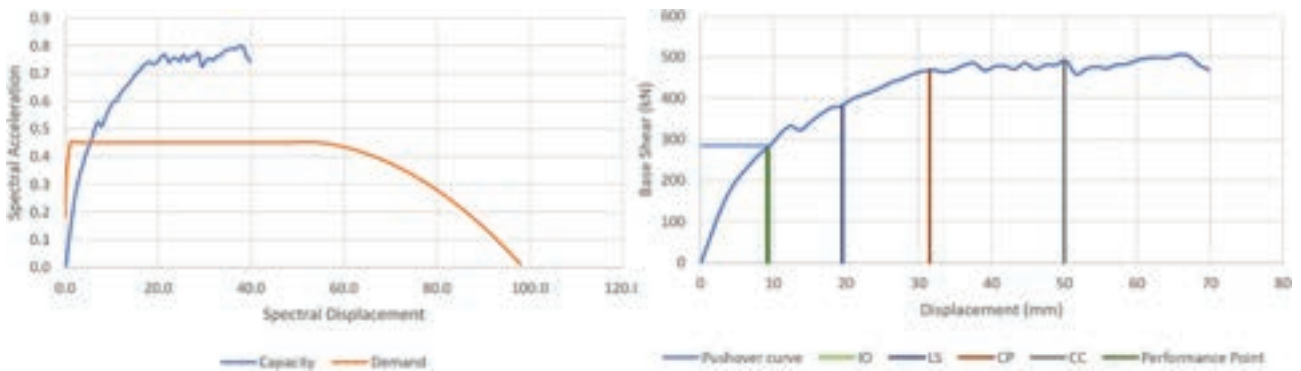


Figure 15: Performance point (left) and performance of the building (right) for 0.18 g PGA

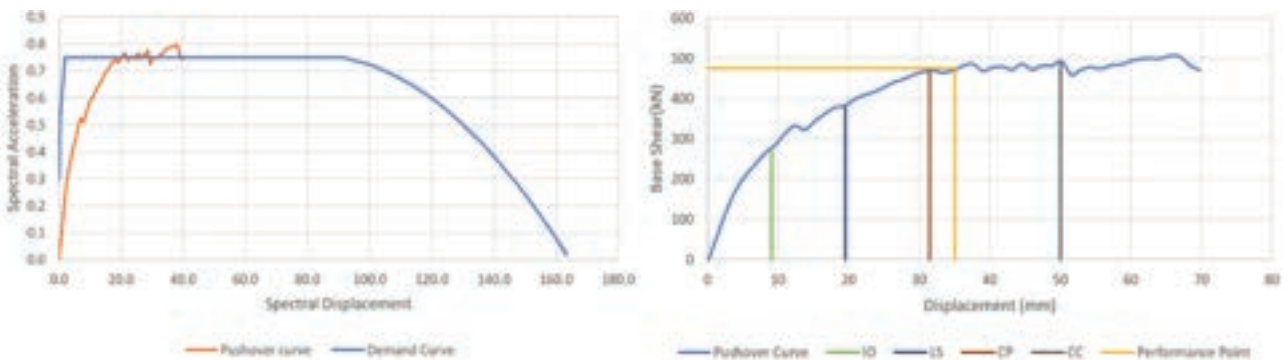


Figure 16: Performance point (left) and performance of the building (right) for 0.3 g PGA

**Table 5:** Performance state of building

PGA	Damage States	Displacement (mm)	Base Shear (KN)
0.15 g	IO	7.02	234.4
0.18 g (for exposed Gorkha earthquake)	LS	9.3	285.077
0.30 g	CC	35.10	475.128

Above figures and table depicts that for 0.15 g PGA, the building imparts immediate occupancy performance level while for 0.18 g PGA, building transit to life safety performance level from immediate occupancy level. Similarly, for 0.3 g PGA performance point lies right of the collapse prevention i.e., building is susceptible to complete collapse at 0.3 g PGA. It also shows that there is rapid increase in damage level when the PGA increases slowly, indicating the relatively brittle failure mode of the building.

### 3.4.1 Performance of gable

The gable significantly affected the capacity curve. The gable is quite flexible in out of plane loading and thus when the control node was selected at top of gable, the stiffness as depicted by capacity curve significantly reduced. Figure 17 compares the capacity curve with and without gable wall.

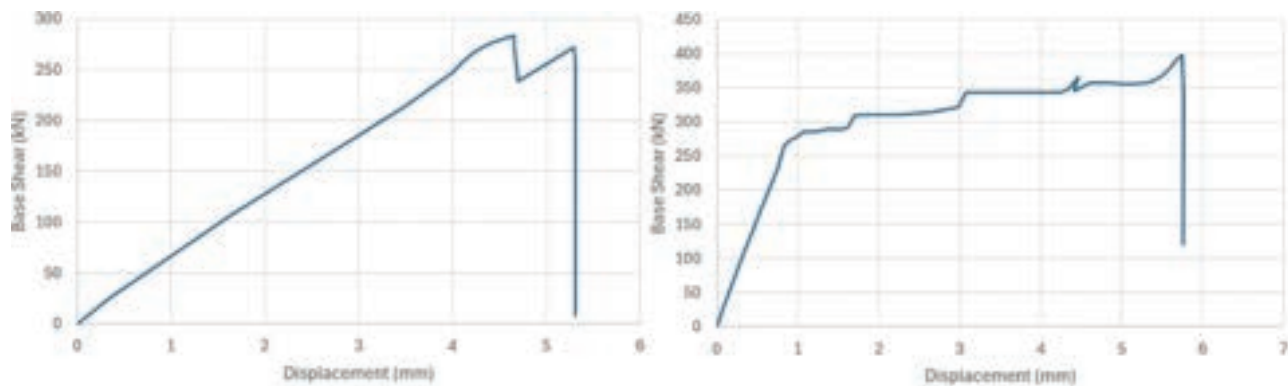


**Figure 17:** Pushover curve of model with gable (left) and without gable (right)

As per Figure 17, displacement is contributed significantly by the gable itself rather than bottom two storey as shown in Figure 18. Brittle collapse was observed at a displacement of 4.7 mm, which is due to collapse of gable. To evaluate the performance of the building other than the gable wall, gable walls were removed from the model and reanalyzed under lateral load to find the capacity curve. Consistent with the capacity curve of the model with the gable, the ultimate force was about 356 kN whereas the ultimate force of 300 kN is observed in the capacity curve obtained from the model with gable walls. However, displacement at that value of load observed in the model without gable is only 1.6 mm. This implies the existence of deformation in the gable resulting in much more early failure of the gable as compared to the rest of the wall. At 0.15 g, the failure of the gable is seen in the PRO\_SAP model. It closely resembles the observed gable collapse at the site during the shaking of about 0.15 g from the Gorkha earthquake as per the shake map provided by United States Geological Survey. To understand the failure mode of other components of the building, further analysis was conducted removing the gable.

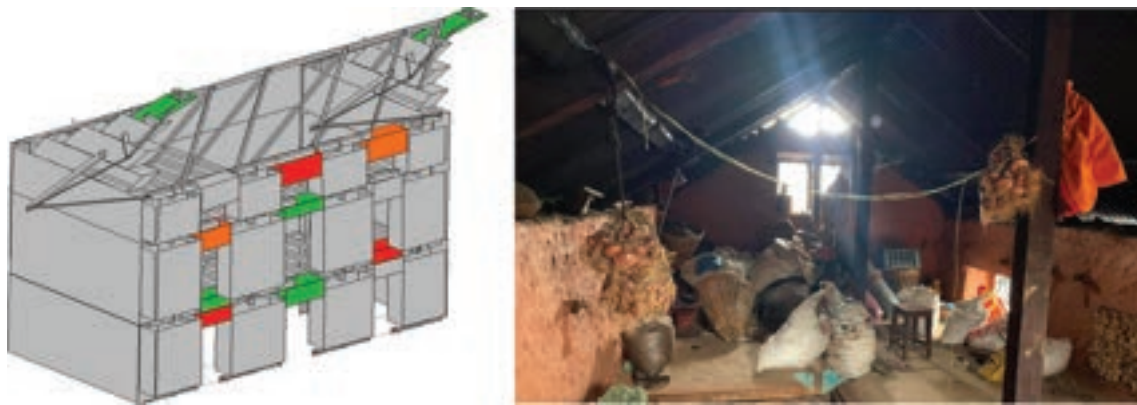


**Figure 18:** Collapse mechanism of Gable wall in EFM (left) and at site (right)

3.4.2 Damage progress

The capacity curve of the building shows that the building has significant non-linear capacity after major yielding at displacement of about 0.85 mm. The ultimate collapse was observed at a displacement of 5.6 mm with ultimate force of 373.1 kN. The damage sequence of the building is discussed. The various types of damage modes in masonry with their adopted histogram colors used in PRO\_SAP (2S.I PRO\_SAP, 2017) is shown in Table 6

**Table 6:** Histogram adopted for damage typology

Damage ID	Histogram color	Damage typology
drO drOo	Red	Excessive drift in the direction parallel to the plane of the wall (drO) or orthogonal to the plane of the wall (drOo) in fully operational limit state
drD drDo	Orange	Excessive drift in the direction parallel to the plane of the wall (drD) or orthogonal to the plane of the wall (drDo) in operational limit state
drV drVo	Yellow	Excessive drift in the direction parallel to the plane of the wall (drV) or orthogonal to the plane of the wall (drVo) in ultimate limit state
drC drCo	Green	Excessive drift in the direction parallel to the plane of the wall (drC) or orthogonal to the plane of the wall (drCo) in near collapse limit state
NM NMo	Blue	Bending moment exceeded bending capacity in the direction parallel to the plane of the wall (NM) or orthogonal to the plane of the wall (NMo)
V Vo	Purple	Shear action exceeded shear capacity in the direction parallel to the plane of the wall (V) or orthogonal to the plane of the wall (Vo)
N	Red	Axial action exceeded tension capacity of the element
N	Blue	Axial action exceeded compression capacity of the element

The horizontal acceleration in the building gradually increased and the performance at major stages are reported to understand the damage patterns. The performance is reported at PGA of 0.065g, 0.14g, 0.19g and 0.35g which correspond to 18.57%, 40%, 54.28% and 100% of design level shaking (DUDBC, 2020). Figure 19 shows that at stage one, even at a small level of ground shaking of PGA 0.065 g, slight tension cracks can be seen in some of the spandrels which appear red in the figure. The spandrels colored green indicates that the bending moment exceeded the bending capacity in the direction parallel to the plane of the wall and the spandrels colored red indicates that the axial action exceeded the tension capacity of the element. In the spandrels, colored orange, the shear action exceeded shear capacity in the direction parallel to the plane of the wall. It has an insignificant effect on lateral capacity of building as observed by the linear capacity curve. At stage two, analysis is carried out for 0.14 g PGA. As shown in Figure 19, shear failure in one of the piers on the first floor represented by an orange-colored pier was observed along with in-plane moment failure of three spandrels represented by the color green.

As shown in Figure 20, at stage three, when the PGA is increased to 0.19 g, almost all front pier in first floor fails in shear while only single pier of ground floor fails in shear. The lateral capacity of the building is further reduced as shown by the reduced slope of the capacity curve shown in Figure 12. However, the building was able to sustain further deformation up to 0.32 g (stage four). Ultimately the building collapsed by an out of plane failure of the wall as shown by the piers colored green in Figure 20. It indicated that the bending moment exceeded the bending capacity in the direction perpendicular to the plane of the wall (out of plane failure) whereas the piers colored orange indicates that the shear action exceeded the shear capacity in the direction parallel to the plane of the wall (in plane failure). It is seen that the shear failure of the ground floor pier is less as compared to the shear failure of the first floor and attic. Shear failure is seen more in the upper story than that on the ground floor. It must be due to the shear enhancement of ground floor walls due to higher compressive stresses and horizontal force distribution from floor system. Also, at first failure, the spandrel occurs, and later the pier begins to fail. Lateral strength is compromised when the pier begins to fail in shear.

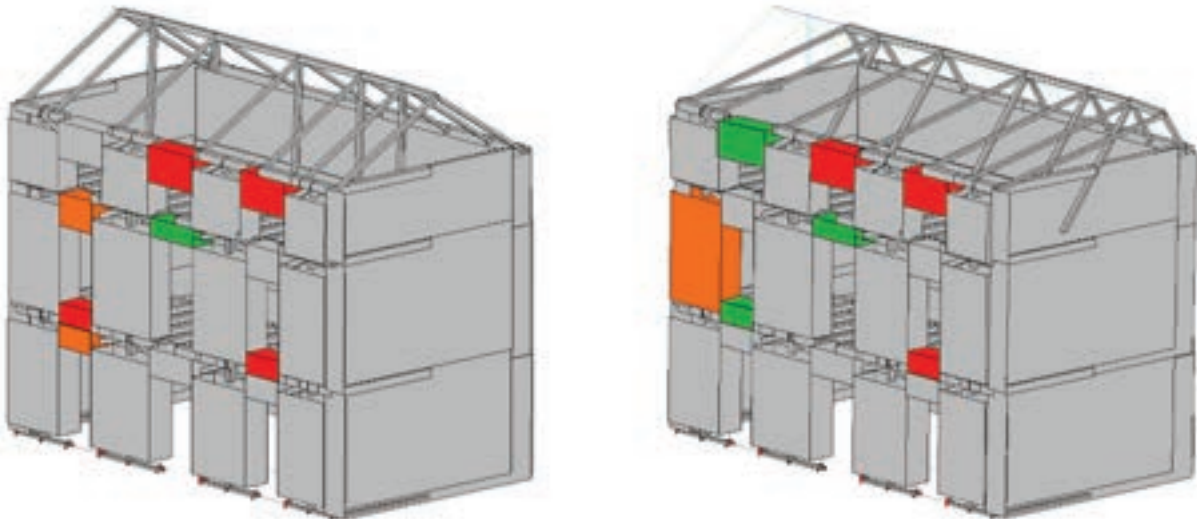


**Figure 19:** Damage pattern at stage1 corresponding to 0.065 g (18.57% of design level shaking) (left) and at stage 2 corresponding to 0.14 g (40% of design level shaking) (right)

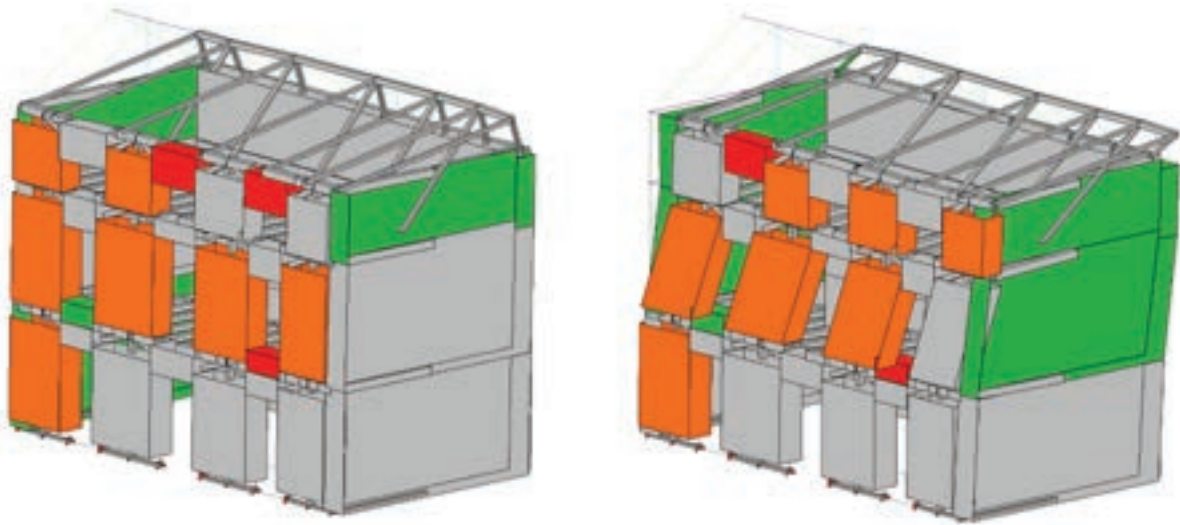


**Figure 20:** Damage pattern at stage3 corresponding to 0.19 g (54.28% of design level shaking) (left) and at stage 4 corresponding to 0.35 g (at design level shaking) (right)

By varying the demand, the corresponding demand for different performance state was also determined as presented in Table 7. The table shows that the building can sustain IO performance state up to 0.15 g, while LS, CP and CC performance state are expected at 0.19 g, 0.30 g and 0.35 g respectively.

**Table 7:** Damage states of the building

Damage States	PGA	Force (kN)	% of ultimate force	Displacement (mm)
Immediate occupancy (IO)	0.15	267.30	71.643	0.8523
Life safety (LS)	0.19	284.40	76.226	1.1
Collapse prevention (CP)	0.30	345.50	92.603	4.4
Complete collapse (CC)	0.35	373.10	100	5.6

The analysis indicates that this type of building can sustain life-safety performance level up to 0.19 g only. However, slight intervention to prevent out of plane collapse of the wall, and avoid masonry unit instability can significantly enhance the performance of this type of building as indicated by large inelastic capacity of pushover curve from FEM.

#### 4. Conclusions

Limited research has been conducted in the past regarding damage mechanisms and dynamic behavior of stone masonry - the most common building typology in Hilly and Himalayan regions of Nepal. Dynamic evaluation of the building showed that stone masonry exhibit wall elasticity of 1256 MPa in ambient vibration. The performance and the damage pattern building components under seismic loading were evaluated in this study.

Linear analysis with FEM showed that this type of masonry building easily satisfies the drift limitation as per NBC code at design basis earthquake. However, significant compressional crushing and tensile cracks

are likely to appear in piers starting from extreme corners of the openings and walls while significant shear cracks are predicted in spandrels and piers of ground and first floor at the design level earthquake although the stresses are just slightly above permissible stress (still below the ultimate strength) at PGA of 0.19 g indicating slight damage of the structure in line with the observed damage during Gorkha earthquake.

From the non-linear static push over analysis using FEM and NBC demand spectra, it is observed that the building attains performance states of immediate occupancy, life-safety, and collapse prevention at peak ground intensities of 0.175 g, 0.250g and 0.295 g respectively, indicating that this type of buildings collapses at design level earthquake of 0.35 g as per NBC.

Similarly, detailed non-linear analysis using EFM showed that the building attains performance states of immediate occupancy, life-safety and collapse prevention at peak ground intensities of 0.15 g, 0.19 g and 0.30 g respectively. Further, the model including the gable wall with control node at gable showed that the control node displacement is contributed significantly by the gable itself rather than lower stories and the gable walls follow a brittle collapse at comparatively lower ground shaking corresponding to 0.15 g PGA. Hence, either of the methods are found competitive in estimating the performance of the masonry building. The predicted damage sequence is also in good agreement with damage observations of similar buildings as reported by (Gautam & Chaulagain, 2016) as well as with the existing damage in the building from 2015 Gorkha earthquake.

## Acknowledgments

The authors acknowledge the Department of Civil Engineering, Thapathali Campus for providing necessary support to conduct this study as a part of BE final year project (2023/24). The authors also acknowledge the field support provided by Er. Bipin Karki for ambient vibration recording. Further, the authors acknowledge the support and generosity provided by the house owner Mr. Netra Prasad Timilsina for the detailed study of the building.

## References

- 2S.I PRO\_SAP. (2017). *PRO\_SAP Reference manual*.
- Adhikari, R. (2023). *Advances in Engineering and Technology Reassessing the seismic compliance issues in relocated settlement after*. 2(1), 103–117.
- Adhikari, R., & D'Ayala, D. (2019). Numerical Seismic Performance Assessment of Pre-Earthquake Stone Masonry Residential Building Typology in Light of 2015 Nepal Earthquake. *In Proceedings of the Society for Earthquake and Civil Engineering Dynamics Conference (SECED), September*, 1–10.
- Adhikari, R., Gotame, S., Regmi, P., Karki, B., & Gautam, D. (2023). Dynamic response of common stone masonry buildings under uncertain material properties. *Journal of Engineering Issues and Solutions*, 2(1), 26–36. <https://doi.org/10.3126/joeis.v2i1.49592>
- Aish, M. Bin, Al-Marwae, O., & Almarwae, M. (2017). *Structural Failure of Buildings: Issues and Challenges*. www.worldscientificnews.com
- ATC 40 Seismic Evaluation and Retrofit of concrete buildings*. (1996).
- Bhochhibhoya, S., & Maharjan, R. (2022). Integrated seismic risk assessment in Nepal. *Natural Hazards and Earth System Sciences*, 22(10), 3211–3230. <https://doi.org/10.5194/nhess-22-3211-2022>
- BIS. (1987a). *IS 875-1 (1987): Code of Practice For Design Loads (Other Than Earthquake) For Buildings And Structures, Part 1: Dead Loads - Unit Weights of Building Material And Stored Materials, Bureau of Indian Standards*.
- BIS. (1987b). *IS 875-2 (1987): Code of Practice for Design Loads (Other Than Earthquake) For Buildings and Structures, Part 2: Imposed Loads, Bureau of Indian Standards*.
- BIS. (1987c). *IS 1905 (1987): Code of Practice for Structural use of Unreinforced Masonry, Bureau of Indian Standards*.
- BIS. (1994). *IS 883 (1994): Design of Structural Timber in Building- Code of Practice, Bureau of Indian Standards*.

- BIS. (2016). *IS 1893 (Part 1) :2016 Criteria for Earthquake Resistant Design of Structures Part 1 General Provisions and Buildings (Sixth Revision)*, Bureau of Indian Standards.
- CSI (Computers & Structures INC). (2016). *CSI Analysis Reference Manual*. www.csiamerica.com
- Dhakal, R. (2020). *System identification and seismic analysis of a residential RC building in Kathmandu, Nepal*.
- DUDBC. (2015). *NBC 202:2015 National Building Code Guidelines on Load Bearing Masonry*, Department of Urban Development and Building Construction.
- DUDBC. (2020). *NBC 105:2020 Nepal National Building Code for Seismic Design of Building in Nepal*, Department of Urban Development and Building Construction.
- FEMA 356. (2000). *FEMA 356, Prestandart and Commentary for the Seismic Rehabilitation of the Building*. FEMA.
- Gautam, D., & Chaulagain, H. (2016). Structural performance and associated lessons to be learned from world earthquakes in Nepal after 25 April 2015 (MW 7.8) Gorkha earthquake. *Engineering Failure Analysis*, 68, 222–243. <https://doi.org/10.1016/j.engfailanal.2016.06.002>
- IAEE. (2014). *IAEE - Guidelines For Earthquake Resistant Non-Engineered Construction*.
- Khadka, B., & Shakya, M. (2021). Seismic characteristics of unreinforced mud masonry houses in Nepal: A miserable scenario before and after 2015 Gorkha (Nepal) earthquake. *Engineering Failure Analysis*, 124. <https://doi.org/10.1016/j.engfailanal.2021.105308>
- Khadka, S. S. (2018). *Seismic Performance of Traditional Unreinforced Masonry Buildings in Nepal*. <https://www.researchgate.net/publication/322977327>
- Kumar Bothara, J., Ahmad, N., Ingham, J. M., & Dizhur, D. (2023). Mechanical properties of stone masonry set in mud mortar and contained by steel wire mesh. *Construction and Building Materials*, 405. <https://doi.org/10.1016/j.conbuildmat.2023.133348>
- Lagomarsino, S., & Giovinazzi, S. (2006). Macro seismic and mechanical models for the vulnerability and damage assessment of current buildings. *Bulletin of Earthquake Engineering*, 4(4), 415–443. <https://doi.org/10.1007/s10518-006-9024-z>
- MIT. (2018). *Norme tecniche per le costruzioni (Technical standards for construction)*.
- NPHC. (2021). *National Population and Housing Census 2021 Volume 01 National report*.
- Paudel, B., & Pradhan, P. K. (2010). Seismic Vulnerability Assessment of Buildings in GIS Environment: Dhankuta Municipality, Nepal. In *The Geographical Journal of Nepal* (Vol. 8).
- Pokharel, T., Pokharel, T., & Goldsworthy, H. M. (2015). *Lessons Learned from the Nepal Earthquake 2015*. <https://doi.org/10.13140/RG.2.1.1657.3528>